Photodissociation of methylnitrite: State distributions, recoil velocity distribution, and alignment effects of the NO(X 2Π) photofragment

U. Brühlmann, M. Dubs, and J. Robert Huber

Citation: The Journal of Chemical Physics **86**, 1249 (1987); doi: 10.1063/1.452214
View online: http://dx.doi.org/10.1063/1.452214
View Table of Contents: http://scitation.aip.org/content/aip/journal/jcp/86/3?ver=pdfcov
Published by the AIP Publishing

Photodissociation of methylnitrite: State distributions, recoil velocity distribution, and alignment effects of the NO ($X\,^2\Pi$) photofragment

U. Brühlmann, M. Dubs, and J. Robert Huber
Physikalisch-Chemisches Institut der Universität Zürich, Winterthurerstrasse 190, CH-8057 Zürich, Switzerland

(Received 2 September 1986; accepted 24 October 1986)

The photodissociation of $CH_3ONO \rightarrow CH_3O + NO$ at 363.9 nm generates vibrationally, rotationally, and translationally excited fragments ($f_{vib}^{NO} = 3\%, f_{rot}^{NO} = 15\%, f_{trans}^{NO} = 33\%$). By means of two-photon LIF and sub-Doppler spectroscopy in combination with various polarization schemes of dissociation and probe lasers, the nascent NO($X\,^2\Pi$) photofragment was characterized with respect to state distributions and three-dimensional recoil velocity distribution. Furthermore, the rotational alignment and the Λ-state populations were determined. Through the rotational alignment dependence of Doppler profiles probed by differently polarized transitions (R and S), the **J**–**v** vector correlation was assessed. Based on these results, stereochemical and dynamical information about the dissociation was obtained which shows that the fragmentation process is planar and takes place within 210 fs.

I. INTRODUCTION

The chemical decay of an isolated, photoexcited molecule has become a research topic of great interest.[1–3] Owing to the laser as a dissociation source and as a spectroscopic tool for fragment analysis, the features of a photodissociation process can be explored in exceptionally fine details. More specific, the application of the laser-induced fluorescence (LIF) technique[4–8] in combination with Doppler spectroscopy[8,9] and the use of various polarization schemes between dissociation and probe laser beams, permit complete characterization of the state distribution and translational energy distribution of the photofragments including their spatial properties such as electron and rotational alignments and fragment anisotropy.

Among the molecules whose photodissociation has recently been investigated in great details by LIF spectroscopy are H_2O,[10,11] H_2O_2,[12] NCNO,[13] HONO,[14] and dimethylnitrosamine $(CH_3)_2NNO$.[15] The latter belongs to the type of polyatomic molecules R–NO that we have been studying in our laboratory for some time,[16] with the NO fragment being analyzed by polarized two-photon LIF.[15] Compared to one-photon LIF, this method is more involved since it requires knowledge of two-photon line strengths of nonisotropic samples in order to transform the measured fluorescence intensities into state populations, but it is more sensitive to the important alignment effects.

Methylnitrite may be photofragmented according to the scheme:

$$CH_3ONO \xrightarrow{h\nu} \begin{cases} \xrightarrow{\text{I}} CH_3O + NO \\ \xrightarrow{\text{II}} CH_2O + HNO \end{cases} \quad (1)$$

Careful TOF measurements[17] have confirmed[18] that after S_1 excitation only channel I is effective, leading to methoxy radical and NO. Recently performed *ab initio* MCSCF calculations of the S_1 potential energy surface of CH_3ONO predict the surface to be dissociative and the exit valley to involve a significant interplay of the O–N and N = O coordinates.[19]

In a previous study, Lahmani *et al.*[20] measured the energy disposal into vibration and rotation of the NO fragment after excitation into various overtones of the N = O stretching mode ν_3 in the S_1 state. The most interesting result concerned the strong vibrational excitation of the NO fragment which increases with increasing higher overtone excitation. The authors interpreted this result as a retention of vibrational energy initially deposited into the N = O stretch of the parent. A similar interpretation might be inferred from the photodissociation data of HONO obtained by Vasudev *et al.*,[14] although these authors discussed their findings with a different model.

In the present study we report on the photodissociation of CH_3ONO at 363.9 nm corresponding to excitation into the 3_0^1 vibronic band of the S_1 state. In contrast to HONO[14] or H_2O_2,[12] which show a quasidiatomic behavior with nearly all of the available energy channeled into translation, the polyatomic molecule CH_3ONO—like the related $(CH_3)_2NNO$ (Ref. 15)—gives rise to a broad energy distribution involving all degrees of freedom. Using the same technique and analysis procedure as in case of $(CH_3)_2NNO$,[15] we obtained an almost complete characterization of the state and translational energy distributions of the NO fragment emerging from excited CH_3ONO. The results provide a detailed picture of the dissociation process of a polyatomic molecule with respect to decay dynamics and stereochemical aspects.

II. EXPERIMENTAL

A description of the experimental set up has been given in a previous publication.[15] In the present experiments, the dissociation laser beam (d) and the probe laser beam (p) were crossed either counterpropagating at an angle of 1.5° or at right angle in a gas cell flowed continuously by CH_3ONO. Both dye lasers were pumped simultaneously with the same excimer laser (Lambda Physik EMG 101 MSC, 308 nm). The probe laser pulse was optically delayed for 10 ns which

 0021-9606/87/031249-09$02.10

was sufficient to establish negligible collisional effects at a sample pressure <150 mTorr. The probe laser (Lambda Physik FL2002E) was operated without étalon (linewidth $<0.2\ cm^{-1}$) to probe the rotational populations and with an intracavity etalon (linewidth $<0.05\ cm^{-1}$) to measure the Doppler profiles. In addition to the previous setup, a thermally stabilized confocal étalon (Tecoptics, finesse 20–30, 400–500 nm) was mounted behind the sample cell to continuously monitor the bandwidth of the probe laser. The dissociation laser was a homemade Hänsch-type dye laser (linewidth $<0.4\ cm^{-1}$). The e vectors of both beams were polarized parallel to the direction of the fluorescence detection. The fluorescence (LIF) of the NO fragment was induced via a two-photon absorption process. Using a Fresnel rotator, the electric vector of the dissociation laser beam e^d was set to $\theta = 0°$ and 90° at each wavelength scanned, where θ denotes the angle between e^d and e^p. The degree of polarization of the laser beams was measured with an additional polarizer (Lambrecht, resolution 10′) and was found $>99\%$ for the dissociation laser beam and $>97\%$ (two-photon process) for the probe laser beam. The intensity of the unpolarized portion of the probe laser beam was too low as to contribute to the two-photon LIF intensity. Saturation effects[6] and power broadening were carefully avoided by keeping the laser pulse energies low, i.e., <2 mJ/pulse and <1 mJ/pulse for the dissociation and probe laser, respectively.

The fluorescence of the NO fragment was detected through a Schott filter set (UV-R-250), with a photomultiplier (Hamamatsu R166UH) which was connected to a four channel gated integrator (Stanford Research Systems, Model SR250). Simultaneously with the LIF signal, the intensities of the laser beams were recorded by means of two photodiodes, allowing an accurate correction for pulse to pulse laser energy fluctuations. The interference signal from the confocal étalon was also fed into the integrator. To accumulate the integrated signals, a Digital Minc 11 laboratory computer was utilized which also controlled the tuning of the probe laser as well as the operation of the Fresnel rotator and the pulse rate (6–8 Hz) of the excimer laser.

CH_3ONO was prepared according to a published procedure.[21] It was purified by several low temperature vacuum distillations.

III. RESULTS

A. Absorption spectrum

The $S_1(n\pi^*) \leftarrow S_0$ absorption of methylnitrite (cf. Ref. 20) is dominated by a progression of the N = O stretching vibration ν_3. The vibronic bands appear to be broadened mainly due to a superposition of the *cis* and *trans* isomers whose absorption bands are slightly shifted with respect to each other.[22] The dissociation laser was set at 363.9 nm which corresponds to excitation of the *cis* form into the 3_0^1 vibronic band. In the ground state the *cis* conformere is more stable by 2.94 kJ/M than the *trans* conformere[23] yielding a molar ratio $[cis]/[trans] = 1.7$. This fact together with the displaced maxima of the *cis* and *trans* vibronic bands justifies the assumption that, using the excitation wavelength given above, a selective excitation of the *cis* form is achieved.

B. Rotational population distribution

Figure 1 shows the two-photon LIF spectrum [$A\ ^2\Sigma^+(v'=0) \leftarrow X\ ^2\Pi(v''=0)$ transition] of the nascent NO fragment after a parent molecule excitation at 363.9 nm. The upper part corresponds to $e^p \| e^d$, the lower one to $e_p \perp e^d$. Under our experimental conditions 12 of the 20 subbranches were resolved. Only clearly nonoverlapping rotational lines were analyzed using the expression for the intensity of two-photon LIF of photofragments[15]

$$I_{fl}(\theta) = K \frac{S^{(2)}(\alpha'',J'';\alpha',\Delta J)}{2J''+1} n(\alpha'',J'') \times [q^{(0)}(J'',\Delta J) + q^{(2)}(J'',\Delta J) \times \overline{A_0^{(2)}}(J'')P_2(\cos\theta)], \quad (2)$$

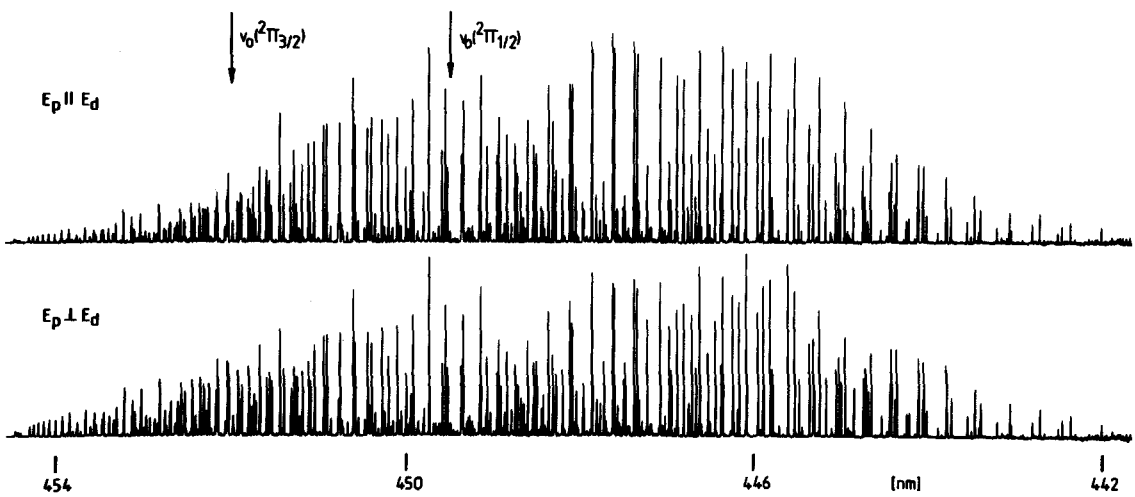

FIG. 1. Two-photon LIF spectra of the nascent NO fragment [$^2\Sigma^+(v'=0) \leftarrow 2\Pi(v''=0)$] after photodissociation of CH_3ONO at 363.9 nm. The upper part shows the recording with probe laser polarization parallel to dissociation laser polarization, the lower part that with perpendicular polarization. The different intensities between these two spectra indicate a significant alignment effect.

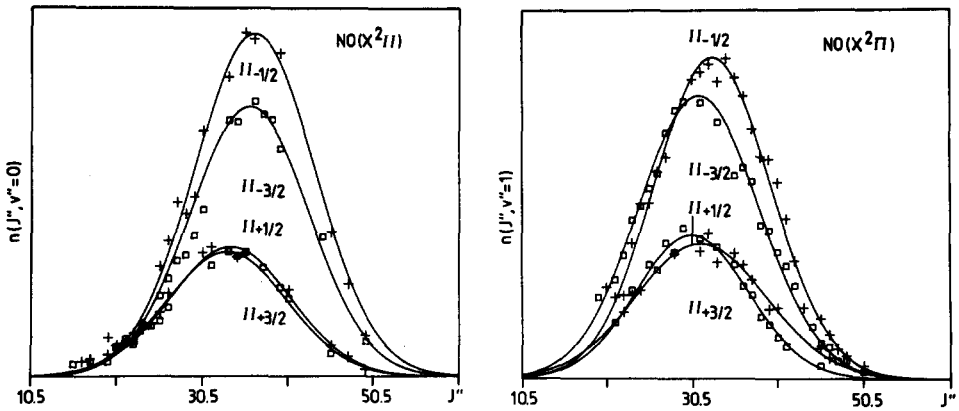

FIG. 2. Rotational state population distributions of the four sublevels in the NO fragment after photodissociation of CH_3ONO at 363.9 nm. The distributions on the left-hand side refer to the vibrational state $v''=0$, that on the right-hand side to $v''=1$. The solid line is a χ^2 fit with a Gaussian-like function.

where $n(\alpha'',J'')$ and $S^{(2)}$ are the population of the probed state with angular momentum quantum number J'' and further quantum numbers α'', and the rotational line strength of two-photon absorption, respectively. The latter was taken from the work of Halpern *et al.*[24] The constant K comprises all fixed parameters such as beam diameters and detector collection angle while $\Delta J = J'-J''$. The bracket term, which describes the angular dependence, contains the molecular alignment $A_0^{(2)}$,[4,5] and the detector polarization sensitivity expressed by the functions $q^{(0)}$ and $q^{(2)}$. The latters were given in a previous publication.[15] $P_2(\theta)=\frac{1}{2}(3\cos^2\theta-1)$ is the second Legendre polynomial with θ being the angle between the dissociation and the probe polarization vector ($\mathbf{e}^d$ and $\mathbf{e}^p$).

The nascent NO fragment is rotationally highly excited ($\langle J\rangle \sim 30$) and can therefore be described by Hund's case (b), the total angular momentum being $\mathbf{J}=\mathbf{N}+\mathbf{S}$ with $\mathbf{N}=\mathbf{R}+\mathbf{L}$.[25] $\mathbf{N}$ and $\mathbf{S}$ are weakly coupled. The singly, unpaired electron in the $p\pi$ lobe of NO gives rise to $L=\pm 1$ so that a nonrotating molecule has $N=L=\pm 1$ and $S=\pm 1/2$. Consequently the various combinations give rise to four states, i.e., the two spin states $F_1(^2\Pi_{1/2})$ and $F_2(^2\Pi_{3/2})$ each of which possesses a Λ doublet $\Pi^+(^2\Pi_{+1/2}, {}^2\Pi_{+3/2})$, and $\Pi^-(^2\Pi_{-1/2}, {}^2\Pi_{-3/2})$. The lower lying F_1 state is separated by $\sim 120\ \mathrm{cm}^{-1}$ [25] from the F_2 state and the Λ states are of different parity. Thus, investigating the Λ states by means of a two-photon transition, the Π^+ states (symmetric with respect to the plane of rotation) are probed via the O, Q, and S branches with the initial levels being F_{1e} or F_{2f}. The Π^- states (antisymmetric) are probed via the P and R branches starting from F_{1f} or F_{2e}. Using the weaker satellite branches, such as ${}^QR_{12}$, ${}^SR_{21}$, the opposite probing scheme applies.

Figure 2 shows the distribution of the rotational state populations of nascent NO in the vibrational levels $v''=0$ and $v''=1$ following dissociation at 363.9 nm. The populations are given for the two Λ-doublet states in each of the two spin states. These distributions are strongly non-Boltzmann. They can be fitted with a Gaussian-type function of the form

$$n(J'') = \text{const}\, e^{-(J''-\bar{J})^2/(\delta J)^2} \tag{3}$$

which is centered at $\bar{J}$ and has a width δJ.

TABLE I. Fragment energy distribution after photodissociation of CH_3ONO at 363.9 nm. (The energies are given in cm^{-1}.) The value E_{weight} of NO is a weighted sum with respect to the vibrational populations ($g_{v=0}=0.75$, $g_{v=1}=0.25$).

	NO ($X\,^2\Pi$)			$CH_3O\cdot$	
	$v''=0, g_v=0.75$[a]	$v''=1, g_v=0.25$[a]	E_{weight} (% E_{avl})	NO($v=0$)	NO($v=1$)
E_{trans}	4750	3950	4550 (33)	4600[c]	3800[c]
E_{rot}, $^2\Pi_{-1/2}$	(0.39)[b]	(0.36)[b]			
$^2\Pi_{-3/2}$	(0.31)	(0.32)	2080 (15)	1200[d]	980[d]
$^2\Pi_{+1/2}$	2150 (0.15)	1750 (0.17)			
$^2\Pi_{+3/2}$	(0.14)	(0.15)			
E_{vib}	0	1880	470 (3.4)	950[e]	1290[e]
E_{el}	50	50	50 (0.4)		
E_{total}	6950	7630	7150 (52)	6750	6070

[a] Vibrational populations according to Lahmani *et al.* (Ref. 20).
[b] Weights according to the rotational population of the four sublevels.
[c] Conservation law $E_{\text{trans}}(\text{NO})/E_{\text{trans}}(CH_3O) = m(CH_3O)/m(\text{NO})$.
[d] Estimation based on the assumption $\mathbf{J}(\text{NO}) = -\mathbf{J}(CH_3O)$, i.e., $E_{\text{rot}}(CH_3O)/E_{\text{rot}}(\text{NO}) \cong B_e(CH_3O)/B_e(\text{NO}) \cong 0.56$.
[e] $E_{\text{vib}}(CH_3O) = E_{\text{total}}(CH_3O) - E_{\text{trans}}(CH_3O) - E_{\text{rot}}(CH_3O)$; $E_{\text{total}}(CH_3O) = E_{\text{avl}} - E_{\text{total}}(\text{NO})$.

Since the rotational distributions conform well with such a Gaussian for all NO states probed, the fitted functions were taken to derive the individual energy contributions of the $^2\Pi_{+1/2}$,$^2\Pi_{+3/2}$,$^2\Pi_{-1/2}$, and $^2\Pi_{-3/2}$ states in the vibrational states $v''=0$ and $v''=1$. To this end the value of the distribution function at a given J'' was multiplied by the corresponding rotational energy as calculated with known rotational constants,[26] and then weighted with respect to the normalized integral of the Gaussian function. To take the vibrational energy distribution into account, the recently reported, relative populations of the $v''=0$ and $v''=1$ states, 0.75 and 0.25, respectively,[20] were used as additional weighting factors. The result is given in Table I. The rotational energy content in state $v''=0$ is $\sim 2150\ \mathrm{cm}^{-1}$, that in $v''=1$ is $\sim 1750\ \mathrm{cm}^{-1}$. Most significant, however, is the preferred population of the Λ state Π^- which shows about twice the population of the Π^+ state at $\overline{J}$. The higher lying spin state F_2 is slightly less populated than the F_1 state; the population ratio $F_1{:}F_2 = 0.54{:}0.46$. The spread of the rotational energy distribution in terms of the FWHM value is 1970 cm^{-1} for $v''=0$ and 1770 cm^{-1} for $v''=1$.

Furthermore, $\overline{J}(F_1) - \overline{J}(F_2) \cong 1$. When n in Fig. 2 is plotted as a function of $N = J \pm 1/2$ instread of J, the rotational populations of the F_1 and F_2 spin states are, within experimental error, identical as has been found in the $(CH_3)NNO$ photolysis.[15]

The Gaussian-like rotational distributions are in agreement with the angular reflection principle for scattering and photodissociation processes.[27] According to this principle, the rotational distribution reflects the Gaussian-like shape of the ground and excited state wave functions. In the case of CH_3ONO, the high rotational excitation of the fragment NO is created via a short lived (<210 fs, *vide infra*) transition state, through the considerable torque caused by the repulsion along the dissociating bond.

The previously published[20] rotational population distributions $n(J'')$ were not corrected for rotational alignment and detector polarization sensitivity. Since these effects are important, as shown below, the $n(J'')$ distributions given by Benoist d'Azy *et al.*[20] are merely approximate and the rotational energies derived from these distributions have to be considered estimations.

C. Population of the Λ doublets

The selective population of one state of a Λ-doublet pair indicates that the $p\pi$ orbital lobe of the NO fragment conserved some of the orientation of the corresponding $p\pi$ orbital in the excited parent molecule just before the dissociation process.[28] A preferential population of the Π^- doublet state implies a parallel orientation of the singly occupied $p\pi$ orbital with respect to **J**. The $p\pi$ orbital is antisymmetric to the plane of rotation of the NO fragment. The Π^+ state, on the other hand, lies in the plane of rotation.[29] The stereochemical implications[29,30] of a selective Λ-state population in the NO photofragment will be discussed below.

As evident from Fig. 2, the Π^- state is significantly higher populated than the Π^+ state. The degree of orbital alignment may be expressed in terms of the population ratio $PR = \Pi^-/\Pi^+$ or the degree of electron alignment

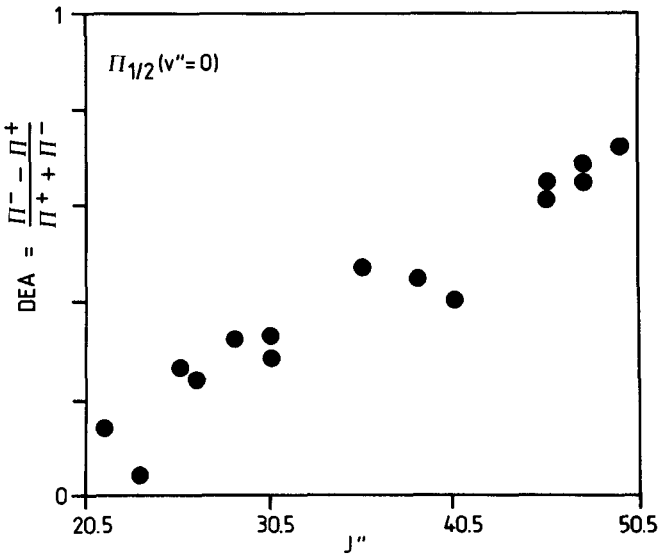

FIG. 3. Population distribution between the Π^- (antisymmetric with respect to the plane of rotation) and Π^+ Λ-doublet states in NO ($X^2\Pi_{1/2}$, $v''=0$) following CH_3ONO photodissociation at 363.9 nm. The distribution is expressed in terms of the "degree of electron alignment" DEA (J'').

$DEA = (\Pi^- - \Pi^+)/(\Pi^+ + \Pi^-)$.[29] A complete electron alignment is achieved when DEA = 1. Figure 3 shows DEA as a function of J'' for the $\Pi_{1/2}$ spin state of the NO($v''=0$) fragment. According to the fit, the highest probed rotational level ($J''=50.5$) furnishes a DEA value of 0.7. Within the experimental error, the same value was found for the $\Pi_{3/2}$ state. This result implies a high degree of electron alignment being close to the theoretical value of 0.8 (NO, $J=50.5$) which is obtained when the expression given by Andresen and Rothe [Eq. (5) in Ref. 29] is applied.

D. Rotational alignment

An anisotropic distribution of angular momenta is measured by means of the polarization behavior of the NO fluorescence. It can be described by alignment parameters $A_\lambda^{(L)}$ which correspond to the multipole expansion terms of the total angular momentum density matrix.[4,5,7,31] In the present case of an initially isotropic ensemble whose molecules are excited with linearly polarized light via a one-photon electric dipole transition, the single parameter $A_0^{(2)}$, i.e., the quadrupole term of the expansion, provides an adequate description of the alignment.

Using two-photon LIF, a bulk value $\overline{A_0^{(2)}}$ can be deduced from the ratio of the fluorescence intensity measured at the angles $\theta = 0°$ and 90° between $\mathbf{e}^d$ and $\mathbf{e}^p$ while keeping all other parameters constant,[15]

$$\overline{A_0^{(2)}}(J'') = \frac{2[I_{fl}(0°) - I_{fl}(90°)]q^{(0)}(J'',\Delta J)}{[I_{fl}(0°) + 2I_{fl}(90°)]q^{(2)}(J'',\Delta J)}. \quad (4)$$

In addition to this straightforward procedure, we also applied the linear regression method and determined the polarization ratio

$$R = \frac{2[I_{fl}(0°) - I_{fl}(90°)]}{I_{fl}(0°) + 2I_{fl}(90°)} \quad (5)$$

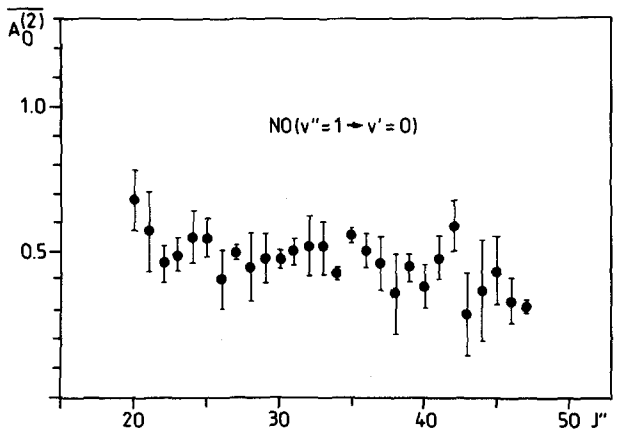

FIG. 4. Rotational alignment $\overline{A_0^{(2)}}(J'')$ of the NO($X^2\Pi$) photofragment obtained from the polarization ratio [Eq. (5)]. The error bars indicate standard deviations.

for different transitions at the same J'' value. The $\overline{A_0^{(2)}}(J'')$ value was then obtained from the linear regression slope of R as a function of $q^{(2)}(J'',\Delta J)/q^{(0)}(J'',\Delta J)$ for each J''. Both procedures gave the same $\overline{A_0^{(2)}}$ value, namely 0.47 ± 0.02 and 0.46 ± 0.02 when the $v''=0$ and $v''=1$ vibrational states were probed, respectively. Disregarding the $\overline{A_0^{(2)}}$ values of the very weakly populated highest and lowest J'' levels displayed in Fig. 4, no significant J'' dependence of the alignment parameter is observed as expected for $J'' > 15$.

E. Doppler line shape and velocity distribution

The Doppler line shape was measured at carefully selected levels $J''=26.5$ in $v''=0$ and $J''=33.5$ in $v''=1$ of the photofragment NO. Each level was probed in the R_{12} and S_{22} branches utilizing the following four configurations of dissociation and probe lasers: $\mathbf{e}^d \| \mathbf{e}^p$; $\mathbf{k}^d \| \mathbf{k}^p$ (case A), $\mathbf{e}^d \perp \mathbf{e}^p$; $\mathbf{k}^d \| \mathbf{k}^p$ (case B), $\mathbf{e}^d \| \mathbf{e}^p$; $\mathbf{k}^d \perp \mathbf{k}^p$ (case C), and $\mathbf{e}^d \perp \mathbf{e}^p$; $\mathbf{k}^d \perp \mathbf{k}^p$ (case D). This gives rise to eight Doppler profiles, shown in Fig. 5, from which we extracted the mean translational energy $\overline{E}_t$, the ΔE_t (FWHM) of the translational energy distribution, and the anisotropy parameter β. The analysis procedure was the same as described earlier.[15] Briefly, for a linearly polarized dissociation laser, the nonisotropic recoil velocity distribution is[32]

$$W(v,\delta) = \frac{1}{4\pi} W(v)[1+\beta P_2(\cos\delta)], \tag{6}$$

where δ denotes the angle between $\mathbf{e}^d$ and the recoil direction and $v = |\mathbf{v}| \cdot W(v)$ is the normalized, and over the angular distribution averaged, velocity distribution. Based on $W(v,\delta)$ and the present conditions, the photofragment Doppler profile is given by[33]

$$G(v_k,\chi) = \int_{|v_k|}^{\infty} dv \frac{W(v)}{2v}[1+\beta P_2(\cos\chi)P_2(v_k/v)]. \tag{7}$$

Here, v_k is the velocity component in the probe beam direction and χ refers to the angle between $\mathbf{e}^d$ and $\mathbf{k}^p$. This expression is then convoluted with the parent velocity distribution and laser line shape to obtain the function which is fitted to

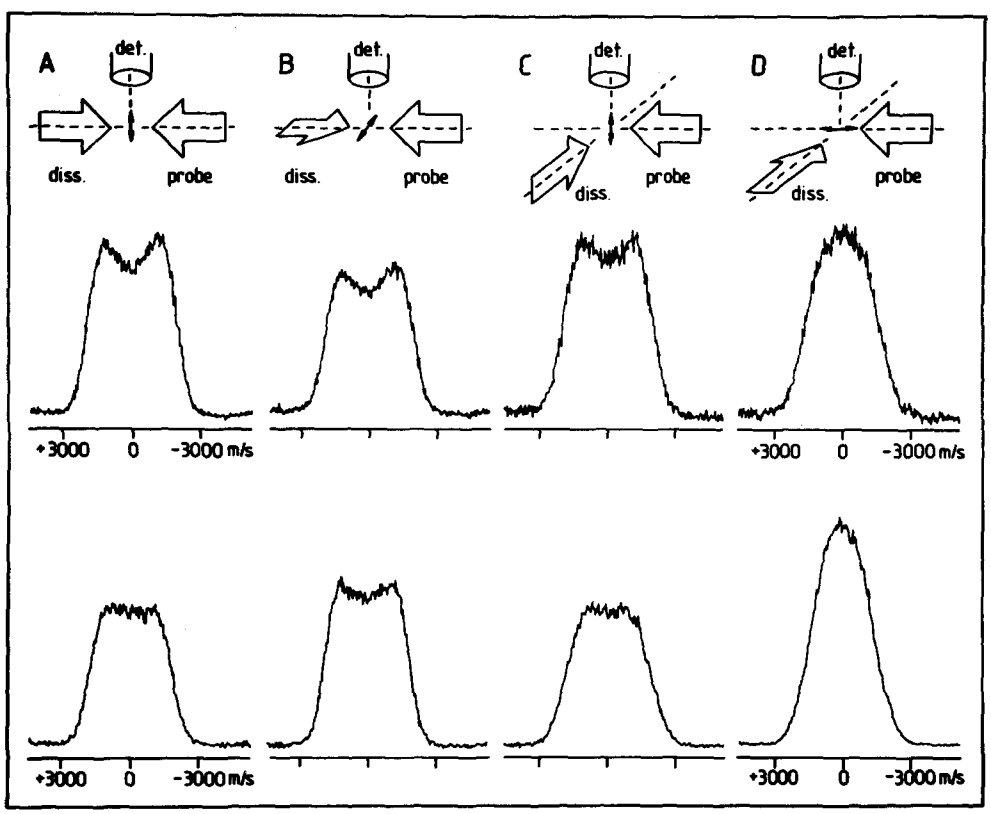

FIG. 5. Measured Doppler profiles of the NO($X^2\Pi$, $J''=33.5$, $v''=1$) photofragment after CH_3ONO dissociation at 363.9 nm using four different geometries for dissociation and probe lasers labeled case A–D (see the text). The upper row shows R_{12}-transition profiles, the lower row those of an S_{22} transition. The abscissa is scaled in units of the velocity component v_k along the propagation direction of the probe laser. (The step size was 5×10^{-5} nm.)

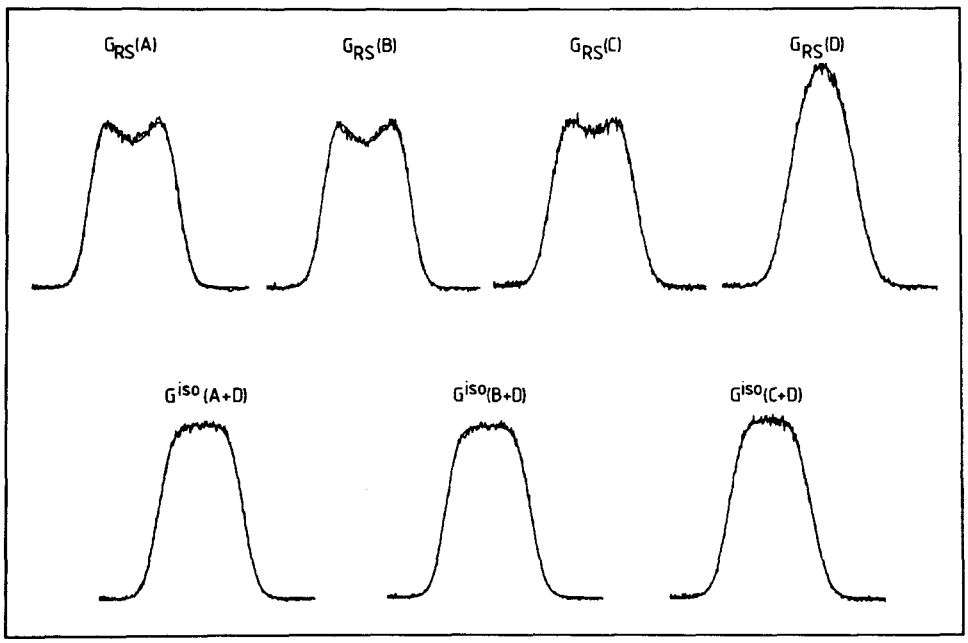

FIG. 6. Corrected Doppler profiles of the NO ($X\,^2\Pi, J'' = 33.5, v'' = 1$) photofragment obtained from the line shapes given in Fig. 5. The upper row shows the profiles after summation of R_{12} and S_{22} profiles according to Eq. (8). The solid line refers to a χ^2 fit providing β (see the text). The bottom row shows the "isotropic" profiles which were derived by summation according to Eq. (9). The solid line represents the χ^2 fit from which $\overline{E}_t$ and ΔE_t was obtained.

the measured profiles of Fig. 5. In a first step, alignment and correlation effects are corrected for and the different Λ-state populations are taken into account, by constructing a properly weighted sum of R and S branch line shapes $G_x(x = R,S)$ according to

$$G_{RS}(v_k,\chi) = w_R G_R(v_k,\chi) - w_S G_S(v_k,\chi). \tag{8}$$

The weights w_x of this normalized function were derived in Ref. 15. The upper part of Fig. 6 exhibits the $G_{RS}(v_k,\chi)$ profiles for the possible combinations.

In a second step β is eliminated by combining two Doppler profiles measured at $\chi = 0°$ and 90°,

$$G^{iso}(v_k) = \tfrac{1}{3} G_{RS}(v_k,0°) + \tfrac{2}{3} G_{RS}(v_k,90°)$$

$$= \int_{|v_k|}^{\infty} dv\, W(v)/(2v). \tag{9}$$

The three "isotropic" profiles thus derived from the four G_{RS} functions are shown in the lower part of Fig. 6.

Instead of differentiating Eq. (9) to obtain $W(v)$, we preferred—out of practical reasons—to simulate the Doppler profile by asserting the previously tested Gaussian-type function[15]

$$W[v(E_t)]/mv(E_t)$$

$$= (\pi\delta^2 E)^{-1/2} \exp[-(E_T - \overline{E}_T)^2/\delta^2 E]. \tag{10}$$

The FWHM is $\Delta E_T = 2(\ln 2)^{1/2}\delta E$. The best fit provided a distribution function $W(v)$ with $\overline{E}_t = 4750\ \text{cm}^{-1}$ and $\Delta E_t = 2130\ \text{cm}^{-1}$ in the $v'' = 0$ state, and $\overline{E}_t = 3950\ \text{cm}^{-1}$ and $\Delta E_t = 1910\ \text{cm}^{-1}$ in the state $v'' = 1$.

Finally the anisotropy parameter β was determined in a separate fitting procedure, using $\overline{E}_t$, ΔE_t, and $G_{RS}(v_k,\chi)$ as obtained by the preceding method. The average value for β probed in $v'' = 0$ and $v'' = 1$ was found to be -0.65 ± 0.05.

F. Correlation between J and v

The fragment rotational motion and the fragment recoil velocity are each correlated with the alignment of the parent molecule transition dipole. Consequently **J** and **v** are correlated with one another. This also implies that the fragment rotational alignment $A_0^{(2)}$ is dependent on **v**. Such a correlation should then be manifested in different Doppler line shapes with different $\overline{A_0^{(2)}}$.[15]

As is evident from Eq. (4), $R(\Delta J = +1)$ and $S(\Delta J = +2)$ transitions have different $\overline{A_0^{(2)}}$ values at a fixed probe/detection polarization [e.g., $A_0^{(2)}(R;J = 26.5)/A_0^{(2)}(S;J = 26.5) = 1.53$ in the $v'' = 0$ state]. Therefore, these transitions should give rise to different Doppler line shapes if an effective **J**–**v** correlation exists. A comparison of the R and S profiles of Fig. 5 clearly shows that such a correlation is present. To express this effect in a more quantitative way we analyzed the profiles omitting the first step of the analysis procedure given above, i.e., we ignored alignment and correlation effects. Thus we fitted the measured Doppler line shapes with the function

$$G_{xx}^{iso}(v_k) = \tfrac{1}{3} G_x(v_k,0°) + \tfrac{2}{3} G_x(v_k,90°), \tag{11}$$

where $x = R$ or S, and obtained $\overline{E}_t$ and ΔE_t for the individual R- and S-branch transitions. The corresponding β values were then obtained by a fit to the $G_x(v_k,\chi)$ Doppler profiles given in Fig. 5. The results are summarized in Table II. The distinctly different values of the parameters for R- and S-branch transitions demonstrate the extent of the **J**–**v** correlation in the NO photofragment.

IV. DISCUSSION

The vibrational structure evident in the $S_1 \leftarrow S_0$ absorption of methylnitrite indicates that the lifetime of S_1 is longer than a vibrational period, $\tau > 3 \times 10^{-14}$ s. The moment μ of the $S_1 \leftarrow S_0$ ($\pi^* \leftarrow n$) transition ($f \sim 0.001$) is perpendicular to the plane of symmetry and localized in the N = O moiety. After the absorption process, the N = O bond is elongated according to a vibrational frequency change from 1610 cm^{-1} in the ground state to $\sim 1000\ \text{cm}^{-1}$ in the S_1 state. The S_1 potential surface, calculated on the MCSCF level, pre-

TABLE II. Effect of the J–v vector correlation measured for the NO ($X\,^2\Pi_{3/2}, v''=1, J''=33.5$) photofragment. $\overline{E}_t$, ΔE_t (FWHM) and β were obtained from χ^2 fits to measured Doppler profiles (Figs. 5 and 6). The mean recoil velocity $v(\overline{E}_t)$ and v were derived from $\overline{E}_t$ and the Doppler width $\Delta\nu_D$, respectively, the latter being calculated from a simple linewidth measurement. The first column gives fully corrected values (see the text), while columns R and S show the values obtained from R- and S-branch transitions ignoring correlation effects. The errors represent statistical errors from several measurements.

		Cases A, B, C	R	S	Error
$\overline{E}_t$	(cm^{-1})	3950	4320	3470	± 130
$v(\overline{E}_t)$	(m/s)	1775	1860	1660	± 50
ΔE_t (FWHM)[a]	(cm^{-1})	1910	1810	1920	± 200
β		−0.65	−0.75	−0.55	± 0.05
$\Delta\nu_D$ (FWHM)	(cm^{-1})		0.297	0.253	± 0.003
$v=c\cdot\Delta\nu_D/(2\nu_0)$	(m/s)		2090	1770	± 20

[a] Upper limit.

dicts the reaction to proceed with an interplay of the O–N and N = O coordinates, releasing the NO fragment vibrationally excited.[19]

A. Fragment energy distribution and lifetime

Since the dissociation energy was found to be $D_0^0 = 14\,500 \pm 400\ cm^{-1}$ [34] and the parent internal energy is $\sim 700\ cm^{-1}$, excitation at 363.9 nm (27 480 cm^{-1}) provides an available energy $E_{avl} = E_0(CH_3ONO) + h\nu_{diss} - D_0^0 = 13\,700 \pm 400\ cm^{-1}$ which is distributed among the internal degrees of freedom and the recoil energy of the fragments, as given in Table I. 65% of E_{avl} is channeled into translation of both fragments. The NO ($X\,^2\Pi$) fragment possesses 33% of E_{avl} as translational, 15% as rotational, 3.4% as vibrational, and 0.4% as electronic energy, respectively. The finer partitioning between the two populated vibrational levels of NO reveals that the vibrational excitation in NO($v''=1$) is partially supplied by E_{trans} and E_{rot}, when compared to NO($v''=0$). The rotational energy distribution among the spin and Λ-doublet sublevels given in Fig. 2 shows the higher population of Π^- relative to Π^+ and the slightly preferred population of the lower $\Pi_{1/2}$ over $\Pi_{3/2}$ (*vide supra*). Moreover, under the assumption of angular momentum conservation, the energy partitioning of the CH_3O fragment into E_{rot} and E_{vib} is presented in Table I.

The prediction of an impact model in its "rigid limit" (i.e., neglect of fragment vibrational excitation)[35] is in fair agreement with the experiment. In terms of E_{avl} one finds 33% and 18% translational and rotational energy, respectively, in NO.

Similar to $(CH_3)_2NNO$,[15] the photodissociation of CH_3ONO, generating rotationally, vibrationally, and translationally excited NO ($X\,^2\Pi$) fragments, furnishes a broad spread of recoil velocities $W(v)$. Neglecting for a moment the small NO vibrational excitation, and assuming angular momentum conservation, the spread of the translational energy distribution of NO corresponds to the vibrational and translational spread in $CH_3O^{\cdot}$. In accord with this expectation the Doppler profile analysis provided a large W(v) width (FWHM) of $\sim 2000\ cm^{-1}$ (2100 cm^{-1} in $v''=0$, 1900 cm^{-1} in $v''=1$).

The anisotropy parameter $\beta = 2P_2(\cos\theta_t)$, where θ_t is a fixed angle between $\boldsymbol{\mu}$ and $\mathbf{v}$, is found to be -0.65 ± 0.05. Its limiting value -1 refers to a perpendicular recoil. Since the contribution of a transverse velocity component of recoil due to parent rotation is only minor ($\sim 1\%$), the observed reduction from -1 can be attributed to parent rotation during the finite lifetime. The average recoil deviation angle is then $|90° - \theta_t| < 20°$. Since the planar dissociation of CH_3ONO (*vide infra*) implies a perpendicular recoil to $\boldsymbol{\mu}$, β provides the upper limit of the lifetime τ of the dissociative state. Following the analysis of Busch and Wilson [Eq. (36)][36] we find $\tau \leqslant 2.1\times10^{-13}$ s for the S_1 state of CH_3ONO excited at 363.9 nm. This lifetime is close to that of $(CH_3)_2NNO$ ($\tau < 2.4\times10^{-13}$ s), being longer than a vibrational period of the N = O stretch (3×10^{-14} s) but shorter than a rotational period of the parent molecule. Keller *et al.*[37] have recently measured the angular distribution of the CH_3ONO in a molecular beam by means of the TOF technique. In agreement with the present result, they found a $\beta = -0.7 \pm 0.05$ for $\lambda_{exc} = 350$ nm.

B. Stereochemical features of the dissociation process derived from rotational and electron alignments

The correlation between the electronic transition moment $\boldsymbol{\mu}$ and J, or in other words the alignment of fragment angular momentum, has found to be in terms of $\overline{A_0^{(2)}} = 0.47 \pm 0.02$. This value is not far from the limiting value of 0.8[4,5] which implies that J is parallel to $\boldsymbol{\mu}$. Thus the dissociation of CH_3ONO populates preferentially large M_i values ($|M_i| \sim |J_i|$) of NO. Since the molecule is planar in the ground and S_1 state with $\boldsymbol{\mu}$ being perpendicular to the plane, this result predicts a dissociation process proceeding in the molecular plane. The reduction of $\overline{A_0^{(2)}}$ from its maximum value can be attributed to parent rotation about the a and b axes (cf. $\beta = -0.65$ instead of -1) and to torsional motions about the internuclear axis O–N. A comparison with the alignments of $(CH_3)_2NNO$ and C_2H_5ONO, $\overline{A_0^{(2)}} = 0.10 \pm 0.05$ ($10 \leqslant J'' \leqslant 35$), and 0.38 ± 0.05 ($15 \leqslant J'' \leqslant 40$),[15] respectively, shows an increasing alignment

with a decreasing size of the molecule. This might simply reflect an increasingly faster dissociation time.

By measuring the relative populations of the Π^+ and Π^- Λ-doublet states, we probed the orientation of the singly occupied $p\pi$ lobe with respect to the NO plane of rotation.[29,30] The strong preference for the Π^- state population observed, indicates a parallel orientation of the $p\pi$ lobe relative to **J**. This $p\pi^-$ orbital is antisymmetric to the plane of rotation of the free NO and the Π^- state correlates with the excited $A''(n\pi^*)$ state of CH_3ONO. Thus the $p\pi^-$ lobe of NO has the same symmetry as the corresponding orbital of the parent molecule implying that the plane of rotation coincides with the plane of the molecule and that the fragmentation process is planar.

After completion of this paper, Lahmani *et al.*[38] published results of a study on rotational and electronic anisotropy of NO following photolysis of CH_3ONO at 355 nm (3_0^2 band). Using the same two-photon LIF technique and analysis method[15] they found $A_0^{(2)} = +0.5 \pm 0.1$ for J'' between 20.5–40.5 in very good agreement with our result. This comparison has, however, to be considered with some caution because the excitation wavelength was different in the two studies. The S_1 potential surface of CH_3ONO was calculated to possess a shallow part in the vicinity of the excitation region[19] which can give rise to product properties sensitive to the excitation energy. The Λ-doublet populations were reported to show a clear preference for the Π^- level but the extent is somewhat different from ours. While Lahmani *et al.*[38] found at $J'' = 40.5$ a ratio $\Pi^-/\Pi^+ \cong 2$ for the F_1 state and ~ 3 for the F_2 state, we obtained $\Pi^-/\Pi^+ \cong 3$ but with no preference for one of the two spin states. Rotational alignment and selective Λ-doublet population indicate also in their work an essentially planar dissociation process. Even in the more complex $(CH_3)_3CONO$ molecule Schwartz-Lavi *et al.*[39] have found a similar stereospecifity upon photodissociation. Thus we may summarize, that the molecules $(CH_3)_2NNO$,[15] $(CH_3)_3CONO$,[39] C_2H_5ONO, and CH_3ONO prefer a planar fragmentation process with respect to the geometry of the main frame (X–O–NO) when excited into the $S_1(n\pi^*)$ absorption.

C. Correlation between J and v

Since our first report on the correlation between the angular momentum anisotropy and the recoil velocity direction observed in the NO photofragment from $(CH_3)_2NNO$,[15] this effect has also been found in the photodissociation of H_2O_2[12,40] and OCS.[41] Dixon has given a theoretical description of the **J**–**v** vector correlation which allows analysis of Doppler profiles for the case of a single recoil velocity.[8] Such an analysis is, however, not yet possible for the complex dissociation process of a polyatomic molecule which possesses a broad recoil velocity distribution of the fragments. Therefore, we assessed qualitative features of the vector correlation obtained through the alignment dependence of the Doppler line shape probing differently polarized transitions (Fig. 5). The effect is expressed by the deviation of the R- and S-Doppler profile parameters from those of a corrected profile (Table II). The result is similar to that found for $(CH_3)_2NNO$, but the correlation is more pronounced in CH_3ONO. Following the arguments given earlier,[15,40] the shape (in particular the dip and wings) of the R- and S-Doppler profiles allows the conclusion that the correlation effect in NO is consistent with preferentially perpendicular **J** and **v** vectors. This perpendicular correlation is not unexpected in view of the fact that the rotational excitation is created by the torque around the c.m. of NO which in turn is generated by the repulsion along the dissociating O–N bond.

V. CONCLUSION

The photodissociation of CH_3ONO at 363.9 nm was studied by probing the internal state and the translational energy distributions of the NO ($X\,^2\Pi$) fragment by means of a two-photon LIF technique. The NO fragment is generated rotationally, translationally, and vibrationally excited, giving rise to broad rotational and recoil velocity distributions. The rotational alignment $\overline{A_0^{(2)}}$, the preferred population of the antisymmetric Π^- Λ-doublet state, the anisotropy parameter β, and the **J**–**v** correlation are consistent with a planar—or almost planar—dissociation process taking place in < 210 fs.

In conclusion, the findings of this photodissociation study show quite clearly that even for a polyatomic molecule such as methylnitrite, the energy partitioning and the stereochemical behavior of the bond breaking process can be highly selective.

ACKNOWLEDGMENTS

Support of this work by the Schweizerischer Nationalfonds zur Förderung der wisssenschaftlichen Forschung is greatly acknowledged. We thank Dr. P. Felder and Professor M. Shapiro for valuable discussions.

[1] W. M. Jackson and H. Okabe, in *Advances in Photochemistry*, edited by D. H. Volman, K. Gollnick, and G. S. Hammond (Wiley, New York, 1986), Vol. 13, pp. 1–94.
[2] J. P. Simons, J. Phys. Chem. **88**, 1287 (1984); S. R. Leone, Adv. Chem. Phys. **50**, 255 (1982).
[3] M. Shapiro and R. Bersohn, Annu. Rev. Phys. Chem. **33**, 409 (1982); G. G. Balint-Kurti and M. Shapiro, Adv. Chem. Phys. **60**, 403 (1985).
[4] C. H. Greene and R. N. Zare, J. Chem. Phys. **78**, 674 (1983).
[5] C. H. Greene and R. N. Zare, Annu. Rev. Phys. Chem. **33**, 119 (1982).
[6] R. Altkorn and R. N. Zare, Annu. Rev. Phys. Chem. **35**, 265 (1984).
[7] D. A. Case, G. M. McClelland, and D. R. Herschbach, Mol. Phys. **35**, 541 (1978).
[8] R. N. Dixon, J. Chem. Phys. **85**, 1866 (1986).
[9] J. L. Kinsey, J. Chem. Phys. **66**, 2560 (1977).
[10] R. Schinke, V. Engle, P. Andresen, D. Hansler, and G. G. Balint-Kurti, Phys. Rev. Lett. **55**, 1180 (1985); A. Hodgson, J. P. Simons, M. N. R. Ashfold, J. M. Bayley, and R. N. Dixon, Mol. Phys. **54**, 351 (1985); M. P. Docker, A. Hodgson, and J. P. Simons, *ibid.* **57**, 129 (1986).
[11] P. Andresen, G. S. Ondrey, B. Titze, and E. W. Rothe, J. Chem. Phys. **80**, 2548 (1984).
[12] K.-H. Gericke, S. Klee, F. J. Comes, and R. N. Dixon, J. Chem. Phys. **85**, 4463 (1986); M. P. Docker, A. Hodgson, and J. P. Simons (to be published).
[13] C. X. Qian, M. Noble, I. Nadler, H. Reisler, and C. Wittig, J. Chem. Phys. **83**, 5573 (1985).
[14] R. Vasudev, R. N. Zare, and R. N. Dixon, J. Chem. Phys. **80**, 4863

(1984); Chem. Phys. Lett. **96**, 399 (1983).
[15]M. Dubs, U. Brühlmann, and J. R. Huber, J. Chem. Phys. **84**, 3106 (1986); M. Dubs and J. R. Huber, Chem. Phys. Lett. **108**, 123 (1984).
[16]R. P. Müller, M. Nonella, P. Russegger, and J. R. Huber, Chem. Phys. **87**, 351 (1984); R. P. Müller and J. R. Huber, J. Phys. Chem. **88**, 1605 (1984); J. Mol. Spectrosc. **104**, 209 (1984).
[17]B. A. Keller, P. Felder, and J. R. Huber, Chem. Phys. Lett. **124**, 135 (1986).
[18]G. Radhakrishna and R. C. Estler, Chem. Phys. Lett. **100**, 403 (1983).
[19]M. Nonella and J. R. Huber, Chem. Phys. Lett. **131**, 376 (1986).
[20]F. Lahmani, C. Lardeux, and D. Solgadi, Chem. Phys. Lett. **102**, 523 (1983); O. Benoist d'Azy, F. Lahmani, V. Lardeux, and D. Solgadi, Chem. Phys. **94**, 247 (1985).
[21]A. H. Blatt, *Organic Synthesis, Collection* (Wiley, New York, 1969), Vol. II, p. 363.
[22]P. Tarte, J. Chem. Phys. **20**, 1570 (1952).
[23]P. Felder, T. K. Ha, A. M. Dwivedi, and Hs. H. Günthard, Spectrochim. Acta Part A **37**, 337 (1981).
[24]J. B. Halpern, H. Zacharias, and R. Wallenstein, J. Mol. Spectrosc. **79**, 1 (1980).
[25]G. Herzberg, *Molecular Spectra and Molecular Structure, Spectra of Diatomic Molecules* (Van Nostrand, Princeton, 1950), Vol. 1.
[26]K. P. Huber and G. Herzberg, *Molecular Spectra and Molecular Structure, Constants of Diatomic Molecules* (Van Nostrand, New York, 1979), Vol. IV.
[27]R. Schinke, J. Phys. Chem. **90**, 1742 (1986).
[28]See, for example, R. P. Mariella and A. C. Luntz, J. Chem. Phys. **67**, 5398 (1977); A. C. Luntz, *ibid.* **73**, 1143 (1980).
[29]P. Andresen and E. W. Rothe, J. Chem. Phys. **82**, 3634 (1985).
[30]M. H. Alexander and P. J. Dagdigian, J. Chem. Phys. **80**, 4325 (1984).
[31]U. Fano and J. H. Macek, Rev. Mod. Phys. **78**, 553 (1973).
[32]R. N. Zare, Mol. Photochem. **4**, 1 (1972).
[33]R. Schmiedl, H. Dugan, W. Meier, and K. H. Welge, Z. Phys. A **304**, 137 (1982).
[34]L. Blatt, K. Christie, R. T. Milne, and A. J. Summers, Int. J. Chem. Kinet. **6**, 877 (1974).
[35]S. J. Riley and K. R. Wilson, Faraday Discuss. Chem. Soc. **53**, 132 (1972); A. F. Tuck, J. Chem. Soc. Faraday Trans. 2 **73**, 689 (1977).
[36]G. E. Busch and K. R. Wilson, J. Chem. Phys. **56**, 3638 (1972).
[37]B. A. Keller, P. Felder, and J. R. Huber, J. Phys. Chem. (submitted).
[38]F. Lahmani, C. Lardeux, and D. Solgadi, Chem. Phys. Lett. **129**, 24 (1986).